Proceedings of Meetings on Acoustics

Volume 20, 2013 http://acousticalsociety.org/

166th Meeting of the Acoustical Society of America
San Francisco, California
2 - 6 December 2013

Session 3aNS: Noise

3aNS5. Acoustic interaction as a primary cause of infrasonic spinning mode generation and propagation from wind turbines.

Kevin A. Dooley* and Andy Metelka

***Corresponding author's address: N/A, N/A, 55 Harbour Square, Toronto, M5J 2L1, Ontario, Canada, kadooleyinc@rogers.com**

Relatively balanced load related pressure waves from the rear surface of each rotor blade, are at a frequency of 1 per revolution of the turbine and are phase shifted by 120 degrees from each other. The superpositions of these infrasonic waves destructively interfere. This action results in a non-propagating rotor locked mode, however, the shielding (reflecting) effect of the tower as each blade passes, interrupts the balanced destructive interference for a small portion of rotor angle three times per revolution. The momentary un-balance between the destructive interfering waves, results in the generation of Tyler-Sofrin spinning mode series, which propagate into the far field. The spinning mode radiation angles, coupled with the low decay rate of infrasound, result in higher far field sound pressure levels than would be predicted for a point source. An analysis approach partially derived from Tyler-Sofrin (1962) is presented. Field microphone data including phase measurements identifying the spinning modes are also presented.

Published by the Acoustical Society of America through the American Institute of Physics

 [DOI: 10.1121/1.4863410]
Received 2 Dec 2013; published 15 Jan 2014

1.0 Introduction

This paper discusses Blade Passing Frequency (BPF) infrasound and its harmonics. Some results on Low Frequency Noise at discrete amplitude modulated frequencies of about 20 Hz plus harmonics, is briefly discussed as a side effect of the spinning mode generation mechanism. This initial analysis focuses on Blade Passing Frequency related noise directly behind (downwind) the turbine. Atmospheric effects on the propagation of spinning modes and noise in general have not been included in this study but will clearly be required for a complete and accurate prediction of far field noise levels.

Other broadband noise generation mechanisms such as vortex shedding or turbulence are not discussed.

2.0 Background

Narrow band infrasonic Fast Fourier Transform (FFT) measurements inside homes situated close to some wind turbine installations show clear acoustic signatures at the BPF and harmonics of the nearby wind turbines (Ref 2, Ref 4). Multiple averaged Fast Fourier Transform (FFT) measurements show similar clearly identifiable acoustic signatures of wind turbine BPF harmonics at over 125 kilometers distance from the closest wind turbine installations (Fig. 8 and Ref. 4) at Sound Pressure Levels (SPL's) which have been measured to be within -25dB of the SPL's recorded inside a home within 500 meters of a turbine installation (Fig. 7 Fig. 8 and Ref. 4). These measurement results spurred an in-depth analysis of the infrasonic noise generation mechanisms involved at the turbine followed by supporting close proximity phase measurements at ground level near (~170 meters) to a wind turbine (Table 1 and Fig. 5).

3.0 Generating Mechanisms

3.1 Rotor locked modes (rotor alone modes)

As has been previously shown by J.M Tyler & T.G Sofrin in their mile-stone paper (Ref. 1), a spinning rotor having a series of airfoil blades in air, produces a rapidly decaying spinning pressure pattern at the rotor, which they named a Spinning Mode. Equation 1.1 of reference 1 is a Fourier series suited to a small diameter uniform flow compressor rotor, and represents the rotor alone mode.

3.2 Wind turbine rotor locked and spinning mode Fourier series

The relatively large radial span of wind turbine blades has the potential for the individual blades being exposed to independently varying aerodynamic conditions during a complete rotation, and as has been detailed in section 5 are certainly subject to independently varying acoustic conditions (Ref. 3). For the above reasons and in anticipation of further requirements to be discussed, the Fourier series representation of reference 1 has been re-defined for this study such that each of the 3 blades on the wind turbine rotor can be treated separately but also as a part of the same rotor system. The re-defined Fourier series includes additional factors which allow for estimates of sound pressure amplitudes at any given axial distance behind the rotor, and also allow for simulation of the tower interference, which results in secondary spinning mode generation (Sec. 4) similar to that described in reference 1, section 6.

$$p\,(\theta,\tau,x) \equiv \sum_{m=1}^{\infty} [\,b_{m_{x_T}}\,\mathrm{p_i}\cos\big(m(\theta_i-\Omega\tau)+\phi_{m_i}\big)$$
$$+\mathcal{F}R_{m_\tau}b_{m_{x_T}}\,\mathrm{p_i}\cos\big(m(\theta_i-\Omega\tau)+\phi_{m_i}\big)]\,S_{m_{x_F}}$$
$$+[\mathcal{F}R_{m_\tau}C_{m_{x_F}}\,\mathrm{p_i}\cos\big(m(\theta_i-\Omega\tau)+\phi_{m_i}\big)-C_{m_{x_F}}\,\mathrm{p_i}\cos\big(m(\theta_i-\Omega\tau)+\phi_{m_i}\big)]$$

$$+\sum_{m=1}^{\infty}[\,b_{m_{x_T}}\,\mathrm{p_{ii}}\cos\big(m(\theta_{ii}-\Omega\tau)+\phi_{m_{ii}}\big)$$
$$+\mathcal{F}R_{m_\tau}b_{m_{x_T}}\,\mathrm{p_{ii}}\cos\big(m(\theta_{ii}-\Omega\tau)+\phi_{m_{ii}}\big)]S_{m_{x_F}}$$
$$+[\mathcal{F}R_{m_\tau}c_{m_{x_F}}\mathrm{p_{ii}}\cos\big(m(\theta_{ii}-\Omega\tau)+\phi_{m_{ii}}\big)-c_{m_{x_F}}\mathrm{p_{ii}}\cos\big(m(\theta_{ii}-\Omega\tau)+\phi_{m_{ii}}\big)]$$

$$+\sum_{m=1}^{\infty}\ [b_{m_{x_T}}\,\mathrm{p_{iii}}\cos\big(m(\theta_{iii}-\Omega\tau)+\phi_{m_{iii}}\big)$$
$$+\mathcal{F}R_{m_\tau}\mathrm{b_{m_{x_T}}}\ \ \mathrm{p_{iii}}\cos\big(m(\theta_{iii}-\Omega\tau)+\phi_{m_{iii}}\big)]S_{m_{x_F}}$$
$$+[\,\mathcal{F}R_{m_\tau}\,C_{m_{x_F}}\mathrm{p_{iii}}\,\cos(m(\theta_{iii}-\Omega\tau)+\phi_{m_{iii}})-C_{m_{x_F}}\,\mathrm{p_{iii}}\cos\big(m(\theta_{iii}-\Omega\tau)+\phi_{m_{iii}}\big)] \qquad 1.1$$

Each of the three terms of (1.1) separated by the Σ symbols represent a single turbine blade designated by the index i, ii, and iii. The blades are located at angles of nominally 2π/3 apart (120 degrees) defined by θ_B ($\theta_i, \theta_{ii}\ and\ \theta_{iii}$) and have effective differential surface pressure values $p_i\ p_{ii}\ and\ p_{iii}$.
An expression for the pressure field of all related tower acoustic interference generated (secondary) spinning mode series (p_S) is given by 2.1, the overall pressure field behind the tower is given by $(p+p_S)$.

$$\begin{aligned}p_S\,(\theta,\tau,x_S,r_S) = S_{n_x}\delta_{x_S}\sum_{n=-k}^{k}&\beta_{n_{m_{x_T}}}\mathcal{F}R_{(m+n)_\tau}\mathrm{b_{m_{x_T}}}\ \mathrm{p_i}\cos\big(m(\theta_i-\Omega\tau)+\phi_{m_i}\big)\\
&+\beta_{n_{m_{x_F}}}\mathcal{F}R_{(m+n)_\tau}\,\mathrm{c_{m_{x_F}}}\ \mathrm{p_i}\cos\big(m(\theta_i-\Omega\tau)+\phi_{m_i}\big)\\
&+\ \beta_{n_{m_{x_T}}}R_{l_{m+n_\tau}}\mathrm{b_{m_{x_T}}}\ \mathrm{p_{ii}}\cos\big(m(\theta_{ii}-\Omega\tau)+\phi_{m_{ii}}\big)\\
&+\beta_{n_{m_{x_F}}}\mathcal{F}R_{(m+n)_\tau}\,\mathrm{c_{m_{x_F}}}\ \mathrm{p_{ii}}\cos\big(m(\theta_{ii}-\Omega\tau)+\phi_{m_{ii}}\big)\\
&+\beta_{n_{m_{x_T}}}R_{l_{m+n_{\psi\tau}}}\mathrm{b_{m_{x_T}}}\ \mathrm{p_{iii}}\cos\left(m(\theta_{iii}-\Omega\tau)+\phi_{m_{iii}}\right)\\
&+\beta_{n_{m_{x_F}}}\mathcal{F}R_{(m+n)_\tau}\,\mathrm{c_{m_{x_F}}}\ \mathrm{p_{iii}}\cos\big(m(\theta_{iii}-\Omega\tau)+\phi_{m_{iii}}\big)\end{aligned} \qquad 2.1$$

(Z_m) :represents the radial location of the center of the pressure pattern at the rotor and (m) is the number of pressure cycles or the rotor harmonic number (Fig. 1).

$$Z_{m_x} = (Z_m + \tfrac{x}{2}) \qquad 3.1$$

$(\lambda_{s_m}) = 4Z_m \sin(\frac{\pi}{2m})$: Representing the circumferential wavelength at the rotor plane 3.2

$r_{x_m} = 0.25\lambda_{s_m} + 0.5x$: Is the radius in a plane of a given pressure wave (m) versus distance (x) 3.3

$A_{x_m} = \pi r_{x_m}^2$ Is proportional to the surface area of the wave-front of mode (m) at distance (x) 3.4

$S_{m_x} = \sqrt{\frac{A_{0_m}}{A_{x_m}}}$: Is the dispersion related decay factor 3.5

$\mathrm{D_{m_x}} = \cos\left(2\tan^{-1}\frac{0.25\lambda_{s_m}}{r_{x_m}}\right)$:Is the destructive interference factor (Sec. 4) 3.6

$b_{m_x} = \sqrt{\frac{A_{0_m}}{A_{x_m}}}\left[1-\ \mathrm{D_{m_x}}\right]$ Combined product decay function (pre tower interference) 3.7

$C_{m_x} = \sqrt{\frac{A_{0_m}}{A_{x_m}}}\cos\left(2\tan^{-1}\frac{0.25\lambda_{s_m}}{r_{x_m}}\right)$ Combined for sum decay function (post interference) 3.8

$\tau = t - [\frac{c}{x_T+x_{F+}\,x_S+r_S}]$ is field real time relative to t which is rotor time (x_S is defined in section 5). 3.9

Ω = 2πN where N is the rotor rotational frequency in Revolutions Per Second 3.10

x_T : is the axial distance between the rotor and the support tower
x_F : is the axial distance between the tower and the far field observation point for rotor locked modes.
p_B : is the blade surface differential pressure on blade B at radius (Z) divided by the highest value of (m) used in the Fourier series calculations (in the cases studied here m < 61).

Equation 1.1 describes the rotating pressure pattern from the rotor plane as a function of time (τ) observer circumferential angle (θ) and distance (x) when the pressure amplitude coefficient (p) is given. The value of (p) is a function of the generator power output, blade design, wind speed, rotor speed, blade angle and radius of the pressure center (Z).

The circumferential pressure distribution implied by the Fourier series of 1.1 for m = 3 only, is illustrated as an example by Figure 1 (left hand side), which is depicting a snapshot of the pressure pattern as it may be observed just rear of the rotor plane of a 40 meter radius wind turbine, the discs representing the Low and High pressure regions (L & H) circumferentially distributed at the ~80% radial location as they may be observed from a rotating, load balanced three blade wind turbine rotor.

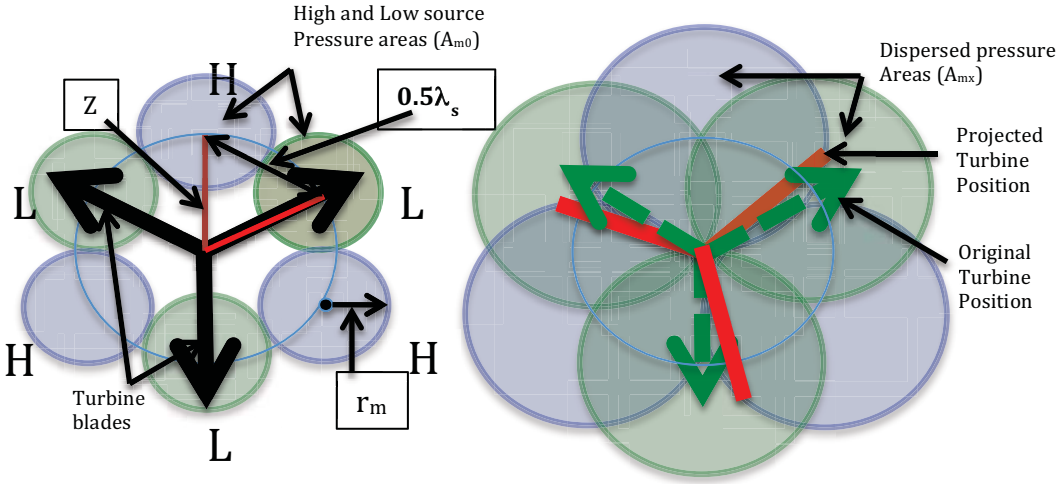

Figure 1

Figure 1 (left side) depicts a snap shot of the pressure pattern at the rotor plane for the fundamental only (m=3); The image on the right is similar and depicts a (spherical) plane rearward from the rotor plane approximately 100mS later (about 34 meters) and illustrates the progressive destructive interference between the highly coherent pressure waves from the rotor as they propagate away from the rotor. Also of note is the increase in the overall diameter of the rotor alone mode relative to the image on the left (rotor plane).

4.0 Open rotor SPL decay rate based on destructive interference (hypothesis)

The decay by destructive interference hypothesis essentially states that the overlap between the circumferentially distributed pressure centers (Fig. 1 right hand image) of a given rotor locked mode (m) will, increase as a function of distance (c * t), which will result in a progressive destructive interference between the pressures centers as a function of distance. This is a result of the angle between the opposing pressure centers being fixed by the harmonic number (m) and the radius at which the mode is located on the rotor (Z_m), however, the angle between the opposing pressure boundaries is a function of the radius of the pressure waves, which is a function of distance and therefor results in a progressive overlapping between the opposing pressure boundaries as a function of distance.

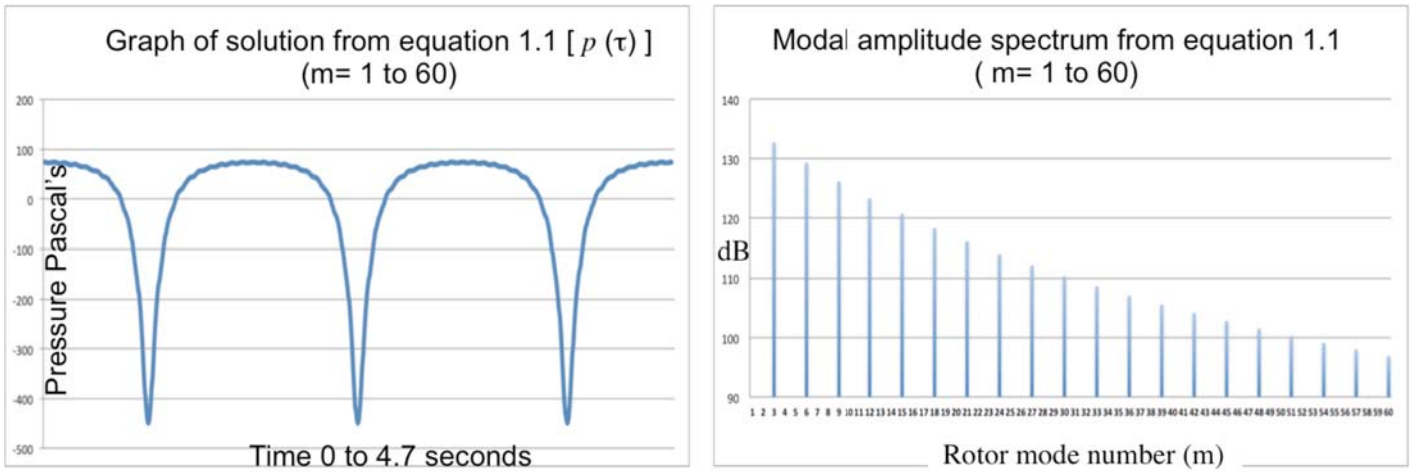

Figure 2

Figure 2 is a time function graph (left) showing the sum of the Fourier series and modal spectrum plot (right) of equation 1.1 for the 3-bladed rotor being modeled, at a distance of 8 m from the rotor plane (i.e. prior to tower interaction). These graphs represent the pressures that would be observed at a single point at a distance of 8 meters rearward from a hypothetical 1.6 MW wind turbine at a radius from the axis (Z) of 32 meters, at rated power based on the preceding hypothesis. Based on the generally accepted primary active radius of the turbine blades being at about 80% of the blade span (Ref. 3) the blade surface Δp is estimated at ~4500 Pa for a 1.6MW turbine. The amplitude coefficient (p) *for (m) = 60, was calculated to be approximately -80 Pa (ignoring wind shear effects which may be accounted for by modulating* $p_i\ p_{ii}$ *and* p_{iii} *as a function of* $(\theta_B - \Omega t)$*).*

5.0 Secondary spinning mode generation

5.1 Tyler Sofrin acoustic reflector interaction

Probably the most significant discovery made in the Tyler Sofrin work was the effect of reflector interaction with the rotor alone modes (Ref 1 Section 6.2 item 3).

The secondary (interaction) modes spin at higher and lower angular rates than the rotor, depending on the number (n) of pressure lobes in the secondary pressure pattern, and is according to the relation $\omega_n = (m\Omega/n)$. This relationship turns out to be important when n<m, because the spin velocity $(Z_n\omega_n)$ will be higher, resulting in some previously decaying modes becoming cut-on when $(Z_n\omega_n) \geq c$, This condition was demonstrated to result in propagation of those particular (cut-on) modes into the far field as opposed to the modes decaying close to the rotor as would be the case without the interaction condition.

It was shown in Reference 1, that for a single interference strut or reflector (as is the case for a wind turbine), $n = mB + k$: where k includes 0, all positive and negative integers $(-\infty < k < \infty)$: k is an integer and B referrers to the number of blades (Ref 1 Section 6.0).

A negative resultant value for (n) indicates a negative spin direction relative to the rotor spin direction.

The frequencies observed for the secondary (interaction generated) spinning modes are identical to the rotor alone mode frequencies since $\omega_n n = m\Omega$, and $m\Omega = 2\pi f_m$.

The interaction phenomenon was demonstrated experimentally during the Tyler Sofrin study and the governing principles are now, and have for some time been widely used in the gas turbine engine and fan industry to reduce radiated noise (Ref. 6).

It is evident that when the tangential velocity $(Z_n\omega_n)$ of any spinning mode pressure pattern C.P. (Center of Propagation: Ref. 1) approaches (c), the circumferential wavelength (λ_s) approaches the free field

wavelength (λ). At this condition, the propagation rate of the rotating pressure pattern in the circumferential direction is identical to the propagation rate in the axial direction (i.e. c). The preceding condition physically prohibits the progressive superposition of the propagating (n) pressure waves, the related hypothetical destructive interference, and the attendant sound pressure level decay. The above set of physical conditions serves as a corollary to the hypothesis related to the SPL decay of the rotor locked modes.

5.2 Wind turbine rotor alone mode tower interaction

The magnitude of the tower reflection is a function of the area of the incident pressure wave (A_{x_m}) 3.4 in conjunction with the intersecting area (profile) of the reflecting tower (A_{T_m}) 4.2, and the repetition duty-cycle; the reflection magnitude is given by:

$$Rl_m = D_T\, A_{T_m}/Z_m 2\pi A_{x_m} \qquad 4.1$$

Where (A_{T_m}): is the common or intersecting area between the tower surface and the pressure wave area (Figure 3), which is approximated by:

$$A_{T_m} = \sqrt[10]{\frac{1}{\left(\frac{1}{A_{x_m}}\right)^{10}+\left(\frac{1}{D_T 2r_{x_m}}\right)^{10}}} \qquad 4.2$$

The Fourier series expression for the attenuation / interference effect (as appears in 1.1) is given by:

$$\mathcal{F}R_m\,(\psi,\tau) = \sum_{m=1}^{\infty} Rl_m \cos\big(m(\psi+\Omega\tau)\big) - Rl_m \qquad 4.3$$

Where:

$\psi = \theta_T - \theta_0$: (θ_T) is the angular location of the tower relative to the observer angle (θ_0)

: D_T is the tower diameter at the radial location corresponding to Z_{m_x}.

Since some portion of each of the pressure waves incident at the tower will be reflected (and scattered) in a forward direction, a pressure proportional to that portion of the wave will effectively be subtracted from the wave traveling past the tower into the far field, resulting in an interference interaction with the un-impeded propagating pressure pattern, including interfering with the destructive interference function responsible for nominally more rapid decay of the rotor locked modes.

The tower reflection Fourier series $\mathcal{F}R_m$ (4.3) forms a stationary pattern relative to the rotor locked spinning pressure pattern, which interferes with the rotating pressure pattern. A rotating interference pattern due to the Vernier effect (due to asymmetry between two similar but non-identical periodic patterns), results from the difference between the stationary attenuation and rotating pressure patterns which is in fact what generates the so called Tyler Sofrin spinning modes (Sect 6.0 of Ref.1).

Some of the spinning modes may rotate with sufficient velocity to attain the cut-on condition as has been previously described and has been demonstrated with other rotor systems (Ref. 1).

The spinning modes having n lobes (p_s) related to the hypothetical wind turbine are given by equation 2.1.

where:

δ_{x_S}	: is an arbitrary decay factor (Sec. 6)
$\beta_{n_{m_x}}$	: is a velocity and radius related coupling factor (4.6, Sec. 6.0)
x_S	: is the axial distance between the observation plane and (x_T)
n	: is an integer where ($-\infty < n < \infty$)
S_{n_x}	: is a decay factor related to the radial distance of the observer from $R_{\beta_{n_m}}$ (Sec. 5.1)

The overall pressure field behind the hypothetical wind turbine is given by;

$p\,(\theta,\tau,x) + p_S(\theta,\tau,x_S,r_S)$: (1.1 + 2.1) Figures 6 and 8 4.4

5.3 ~20Hz + harmonics Amplitude Modulated products.

It is highlighted that a portion of the pressure wave reflected forward from the tower will be incident to the passing blade surface, which results in a portion of the wave reflecting back toward the tower, resulting in a (somewhat inefficient) periodically excited resonant space (Fig. 4). Scale measurements on a 1.6 MW turbine results in the distance between the blade and tower estimate at about 8.5 to 9.0 meters at the ~80% blade radius, which varies slightly as wind loading forces the blade towards the tower at higher wind speeds or power levels. The gap between the two reflecting surfaces form a half wave resonator when the blade is close to the tower, for frequencies of about 20Hz, 40Hz etc. and will result in some acoustic emission of these frequencies (Fig. 7) in conjunction with upper and lower sidebands at the BPF (the resonance is excited intermittently at the Blade Passing Frequency causing Amplitude Modulation and probably some Frequency Modulation of the resonance). The reflection coefficient (Rl_m) predicts a 46dB reflection amplitude from the tower for m= 84 (20.1 Hz) and about 30db for m =168 (at rated power and wind speed), volumetric displacement effects of the moving blades will tend to increase the predicted pressure wave magnitude locally, however, these effects are not as yet included in the model. The resonance amplification factor has not been evaluated.

The amplitude-modulated resonance will also result in some axial vibration (at the 20Hz + harmonics resonant frequencies) of both the tower and the turbine blade as the blade passes the tower.

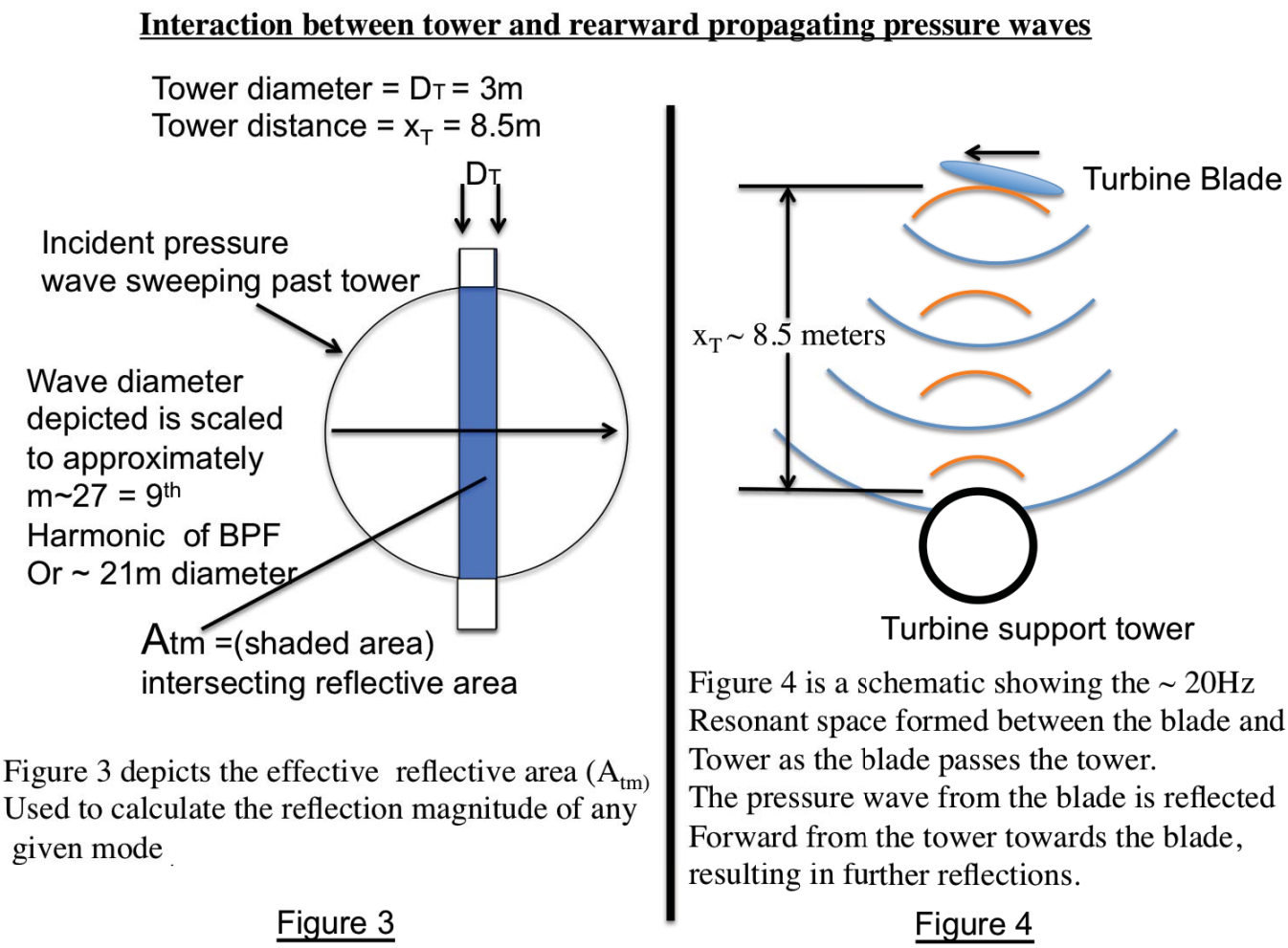

Figure 3 depicts the effective reflective area (A_{tm}) Used to calculate the reflection magnitude of any given mode

Figure 3

Figure 4 is a schematic showing the ~ 20Hz Resonant space formed between the blade and Tower as the blade passes the tower. The pressure wave from the blade is reflected Forward from the tower towards the blade, resulting in further reflections.

Figure 4

6.0 Spinning Mode Radius Physical Limitation

Evidently the maximum physical radius possible for any propagating spinning acoustic mode is limited by the speed of sound (c) in the medium of propagation and is defined here as the propagation radius (R_β):

$$R_{\beta_{n_m}} = \frac{nC}{2\pi \mathrm{N}m} \qquad 4.5$$

Where: (n) is the number of spinning pressure lobes, (c) is the local speed of sound and Nm is the frequency in the stationary frame.

It is also evident from Reference 1 and the previous discussions of this study that there can be no sustained axial propagation of a spinning mode when the radius of its C.P. is less than the propagation radius (i.e. the mode is not cut-on and therefor decays). These two demonstrable features[*1] of spinning modes, imply a fixed and well-defined radius of propagation ($R_{\beta_{n_m}}$) for any given propagating spinning mode (p_s). These two assertions imply that no distance related normal dispersion (Ref. 5) of the pressure waves could be predicted.
Although no experimental measurements have been made in this study to confirm the propagation radius hypothesis, the computed radiation patterns of reference 1 (Fig. 20 of Ref. 1) and measurement data presented (Figures 21A and 21B of Ref. 1), support the hypothesis by showing the radius of the measurable SPL near the duct face, reducing as an inverse function of cutoff ratio ($\mathcal{E}$): where ($\mathcal{E}$) $= \frac{M^*}{M}$: $M^*$is the mode CP Mach number (This is demonstrated most clearly by conversion of the polar plots of figure 21 Ref. 1 into rectangular coordinates based on Fig 19 of Ref 1. The authors of Ref. 1 did not note this relationship).

6.2 Near field phase measurements

Phase measurement data recorded at close proximity to a wind turbine at ground level, which are presented in table 1, indicate phase angles between a pair of microphones (two sets of microphones were used) placed 50 meters apart, ~170 meters behind a wind turbine, approximately parallel to the rotor plane (shifts in the wind direction during the recordings will have resulted in errors in the parallelism of the microphone setup which was not measured during the recordings).
The setup for the phase measurements is shown in Figure 5.

6.3 Spinning mode coupling coefficient

It follows that if there is no acoustic energy incident at the propagation radius (R_β) of a particular interaction (interference) generated spinning mode, no propagating spinning mode could be established.
For example no propagating spinning mode results if $(Z_{m_x} - r_{m_x}) > (R_{\beta n})$, that is the innermost radius of the rotating input pattern being greater than the propagation radius $(R_{\beta n})$. Or if $(Z_{m_x} + r_{m_x}) < (R_{\beta n})$ for resultant interaction modes. However, more research on the effect of an increasing $(Z_{m_x} + r_{m_x})$, as a function of distance is required to ascertain whether dispersion related radial expansion, results in an eventual cut-on condition and a propagating spinning mode (Sec. 7).
The second coupling limit $(Z_{m_x} + r_{m_x}) < (R_{\beta n})$ occurs for our hypothetical wind turbine when m < 5. This limitation prevents the BPF (m=3) from ever becoming a propagating interaction spinning mode. This fact may explain the noted absence of the fundamental BPF in measurements by at least 1 observer (Ref. 4 & Fig. 8).
A resonant-like unity gain, coupling coefficient ($\beta_{n_{m_x}}$) has been formulated based on the energy availability at the propagation radius ($R_{\beta_{n_m}}$) and is incorporated into the expression (p_S) 2.1 representing the interaction spinning modes. ($\beta_{n_{m_x}}$) 4.6 is a convenient method to filter out non-propagating interaction spinning modes from the results of (2.1), and is given by:

$$\beta_{n_{m_x}} = \frac{r_{m_x}}{\left(Z_{m_x} - R_{\beta_{n_m}}\right)^2 + r_{m_x}} \qquad 4.6$$

6.4 Interaction spinning mode decay rate

The decay rate of sub-sonic spinning modes (the rotor alone modes for example) is governed by a combination of dispersion (spherical spreading) and destructive interference, both of which are active features in the decay of the rotor alone modes. The decay rate of free field sonic spinning modes appears to be in question, since the propagation radius cannot increase without violating the sonic velocity limit. This constraint appears to discount spherical spreading and its related SPL decay as it is presently defined. The SPL measurements made at 125 Km distance tend to support this hypothesis (Figure 8 and Ref. 4). The progressive destructive interference between wave fronts in a given pattern in the direction of propagation is also eliminated since the propagating spinning modes in any given mode from a single turbine are mutually coherent (sourced by the same rotor system) and are all propagating at the same velocity.

It is not reasonable to expect that there will be zero decay in SPL of a spinning mode, pending further research in this area, and for the purpose of this study, an arbitrary decay function (δ_{x_S}), which is an exponential function of time, has been assumed. A second assumption is that there will be some radiation of infrasound from the spinning mode in a radial direction forming an Archimedean Spiral, which is expected to decay as a function of radial distance from the mode radial location $R_{\beta_{n_m}}$ as a line source. This assumption is supported by the phase measurement results tabulated in table 1.

$\delta_{x_S} = e^{-\left(\frac{x_S}{kc}\right)}$ is an arbitrary axial exponential decay factor 4.7

Where: k is a time constant, which based on extreme far field data has been set at 120 seconds.

$\left(S_{n_x}\right) = \frac{.5\lambda_n}{r_S + .5\lambda_n}$ where (r_S) is the radial distance from the mode radius $(R_{\beta_{n_m}})$ 4.8

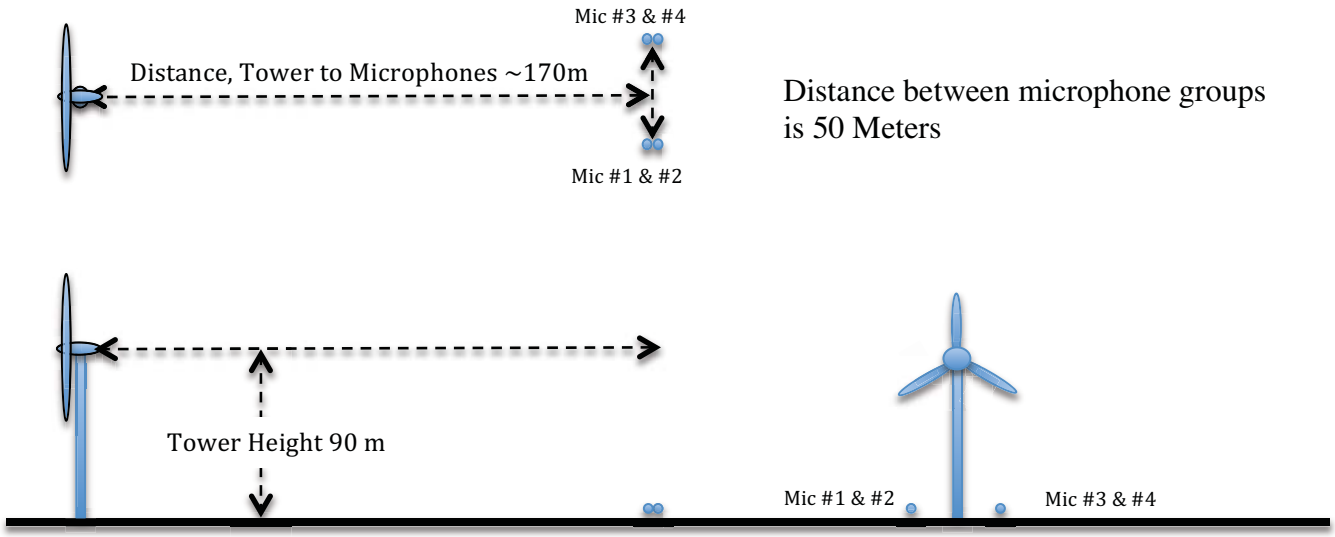

Figure 5

Frequency	Rotor Mode (m)	ϕ Mic # 2 Degrees	ϕ Mic # 3 Degrees	ϕ Mic # 4 Degrees	Average ϕ (3 & 4) - (1 & 2)	Calculated lobe (n) = ϕ / A	Ideal ϕ (for -n)	Error %	$R_{\beta_{n_m}}$
0.72 Hz	3	1.269	+92.70	+96.17	+93.16	-3.0 (3)	+93.12	0	225m
1.44 Hz	6	-2.648	+134.22	+136.5	+136.7	-4.4 (4)	+124.16	+10	150m
2.16 Hz	9	-2.480	+129.34	+129.82	+130.8	-4.2 (4)	+124.16	+6.6	100m
2.88 Hz	12	-0.825	+118.42	+121.38	+120.3	-3.87 (4)	+124.16	-3.8	75m
3.6 0Hz	15	-2.403	+162.00	+164.44	+164.4	-5.29 (5)	+155.2	+5.9	75m
4.32 Hz	18	-4.289	+121.11	+120.34	+122.5	-3.9 (4)	+124.16	-1.3	50m

Table 1.0

Phase Measurement Results and Calculated Spinning Mode lobe numbers (n)

The angle (A) of table 1 is the physical angle formed between the axis of the turbine and the two microphone sets (Fig. 5). $(A) = 2\arctan\left(\frac{25\ meters}{90\ meters}\right) = 31.05$ Deg.

The phase angle Average (ϕ) of table 1 is the average phase measured between the reference microphones (1 & 2) and microphones (3 & 4). The detection of these phase angles is supporting evidence for spinning mode generation.
All mode phase polarities (phase of 3&4 are leading 1&2) indicate that the detected modes are counter-rotating modes (n< 0), since the rotor rotation is in a counter-clockwise direction looking from the rear of the turbine from the microphones location, whereas the rotation of the modes indicated by the phase polarity is clockwise. This confirms interaction spinning mode generation.

None of the detected spinning modes at ground level are calculated as being cut-on at the interaction zone radius of ~ 40 meters (i.e. $R_{\beta_{n_m}} > 40$ meters). That the magnitude of phase angles is measurable at the radius of measurement may be explained by either the assumption that decaying interaction spinning modes transition to an Archimedean spiral radiation pattern only, or that decaying interaction modes cut-on at $(R_{\beta_{n_m}})$ and also radiate in an in Archimedean spiral radiation pattern from the $(R_{\beta_{n_m}})$ radius. Further research and measurements are required with respect to near to cut-on spinning modes to formulate a more complete theory.

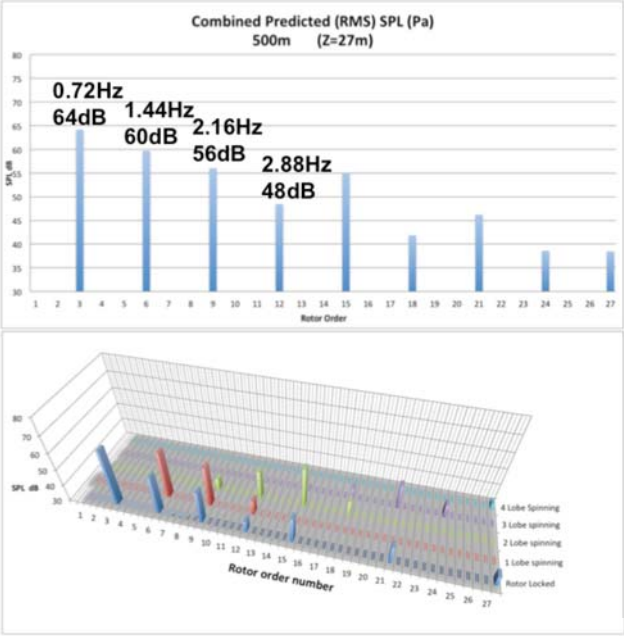

Figure 6

The upper image of Figure 6 are results of Equ. 1.1+ Equ. 2.1 at an (x_F), (x_S) =500m , (r_s) of 90m and θ = 0. The lower image shows results of 1.1 and 2.1 separated into Rotor locked modes (front row), and one lobe, two lobe and three lobe modes. the best agreement with the measured trends (Figure 7) was obtained using 27 meters (68%) as the pressure center on the rotor Z_m as opposed to 32m (80%)

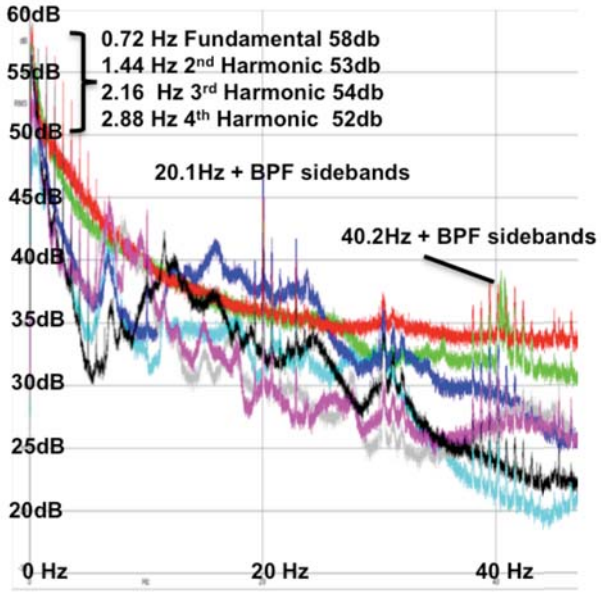

Figure 7

Figure 7 above, is an un-weighted SPL recording made in Kincardine Ontario in July 2013, over-night (Ref 4).
The Red and Green traces are outside microphones ~400 and ~500 meters from a 14.4 RPM 1.6 MW rated wind turbine. Blade passing harmonics and 20.1 Hz amplitude modulated harmonic series are prominent in the Frequency Spectrum. The operating power level is un-known.

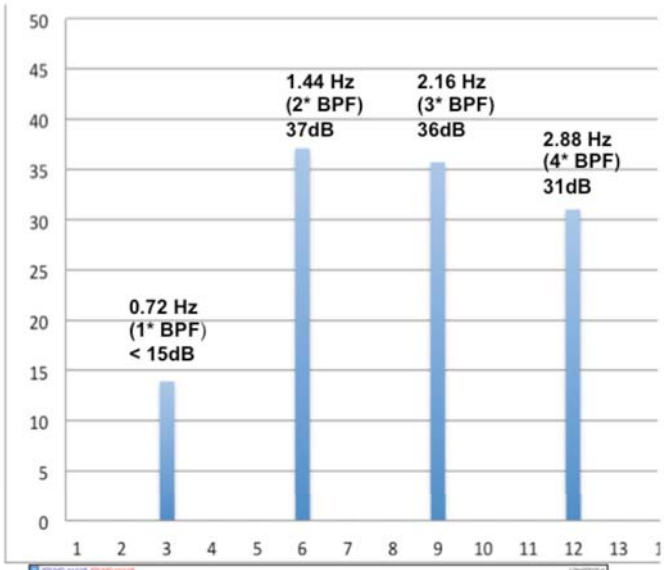

Extreme Far Field Predictions versus Measured results for the first 4 Fourier Components BPF, 2nd 3rd and 4th harmonics (3rd, 6th, 9th and 12th rotor orders).

The data displayed to the upper left are the results from equation 1.1 + equation 2.1 at a distance (x_F and x_s) =125 Km, (r_S) = 90m, with an assumed turbine power at the rated power of 1.6 MW.

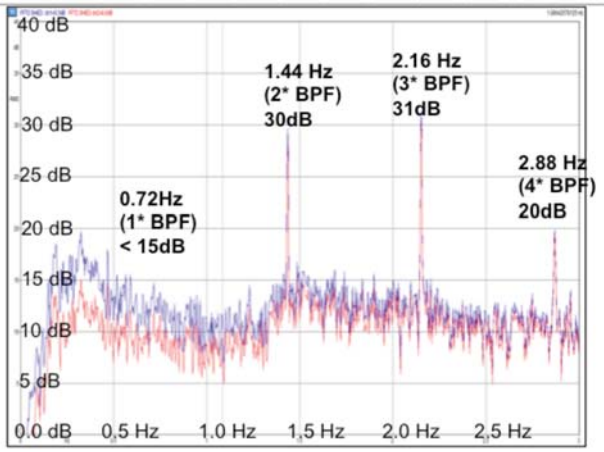

The recording displayed to the lower left is of two microphones recorded together in July 2013 in Parry Sound Ontario, which is over 125 Km from the closest wind turbine (Ref. 4). It is not known what power level the remote turbine was operating at.
Of note is the low level of the BPF component relative to the second and third harmonics. According to the hypothesis and the model presented. the BPF mode is not predicted to generate a spinning mode, thus the spinning mode components are expected to be of significantly higher SPL than the BPF in the far field

Figure 8

Figure 8 (upper) is based on the same parameters as Figure 6 results, except that the axial observation distance (x_F and x_S) has been increased to 125 Kilometers. The amplitude decay of the rotor locked modes is very significant with the BPF reduced by about 50db and harmonics of the BPF rotor locked modes decaying by more than this. The spinning modes are predominant because no spherical spreading or destructive interference decay is predicted in this model, with only an arbitrary time function exponential decay included. The data in the combined amplitude plot of Figure 8 upper, compares favorably with data recorded ~125 Kilometers from the closest wind turbine in Parry Sound, Ontario (Fig. 8 lower & Ref. 4). Of particular interest is the agreement on the very low magnitude of the 3rd order mode (BPF) which can not attain a cut-on condition through interaction, since a single lobed mode at the BPF will only spin 3 times the rotor speed (Sec. 5), the base rotor speed center of pressure velocity, is less than Mach 0.15 and as such would need to increase by a factor of at least 6 for any portion of the mode to achieve a cut-on condition.

*[1] *The concept related to an upper radius limit* ($R_{\beta_{n_m}}$) *was not discussed in Ref. 1, however the concept of a limited radius presented here is in full agreement with Ref. 1 formulations. This can be shown if one considers a case where the Ref. 1 duct radius is just less than* ($R_{\beta_{n_m}}$) *limiting the radius of the mode to less than* ($R_{\beta_{n_m}}$) *where axial propagation of the spinning mode rapidly decay's. Increasing the radius of the duct beyond* ($R_{\beta_{n_m}}$) *for precisely the same rotor conditions, will allow the same mode to propagate in the axial direction essentially un-attenuated based on Ref. 1 calculation methods. This can be confirmed through the formulations of Ref. 1 where the circumferential wavelength was derived as* $\lambda_s = \frac{2\pi r_0}{m}$*: where* ($r_0$) *is duct wall radius and (m) is the number of pressure lobes in the circumferential pressure pattern.*

7.0 Summary

The fundamental process through which the generation of spinning modes from a hypothetical wind turbine are generated, has been examined and formalized through the application of Fourier series.

A hypothesis, which proposes an explanation for the rapid decay of rotor locked modes while simultaneously explaining the generation of propagating spinning modes by acoustic interference, has been presented.

The source of low frequency noise (~20 Hz AM harmonic series) commonly measured near wind turbines is predicted as being a side effect of the spinning mode generation process, the mechanism described may suggest potential amplitude reduction techniques for the resulting 20 Hz harmonic series LFN.

Data which has been generated using the hypothesis and related equations presented, compares favorably to close range measurements shown in this study, and in measurements made by others (Fig 6, Ref 2 and Ref 4), and with measurements made at over 125 Km from the closest wind turbine (Fig. 8 and Ref. 4).

A concept related to a limited and specific propagation radius of acoustic spinning modes based on the speed of sound (c) has been presented. The trend of data available in Ref. 1 (figure 21A and 21B) supports this concept when the referenced data is interpreted using polar to rectangular coordinate conversion.
The concept indicates that the SPL decay rate of propagating spinning modes is less than what would be predicted from a point source based on either spherical or cylindrical spreading at similar frequencies. However, extreme far field levels may not yet be accurately predictable. Further research is required to better formulate the SPL decay characteristics of low frequency free field spinning modes with respect to dissipation and atmospheric influences.

Phase measurement data presented in Table 1 indicates that interaction spinning modes are generated, and that none of the spinning modes measured at ground level would be cut-on modes at the interaction zone radius. The phase measurement data raises the question as to the nature of the decaying spinning modes transition through ($R_{\beta_{n_m}}$) as a result of spherical spreading. The ~90m radius of the phase measurement location is > ($R_{\beta_{n_m}}$) for the 4th 5th and 6th harmonic of BPF, the magnitude of the phase angles detected between the microphones at the measurement radius, indicates that these spinning modes are in the form of an Archimedean spiral pattern.
Evidence that the decaying spinning modes also achieve a cut-on condition as they attain the propagation radius ($R_{\beta_{n_m}}$) as a result of spherical spreading (i.e. due only to the increase in Z_{m_x}) has not been documented, however this phenomenon has not been ruled out.

ACKNOWLEDGEMENTS

The encouragement and many useful suggestions from Professor Colin Hanson and my colleague and friend Tatjana Pekovic in the preparation of this report were invaluable.
The many hours of stimulating and challenging discussion with my friend, business partner and colleague Mr. Elwood Morris will pay dividends for many years to come.

REFERENCES

[1] J. M. Tyler and T. G. Sofrin "Axial Flow Compressor Noise Studies," SAE Technical Paper 620532, 1962, doi:10.4271/620532.

[2] B. Walker, G.F. Hessler Jr., D. M. Hessler, R. Rand, P. Schomer. "A cooperative measurement survey and analysis of low frequency and infrasound at the Shirley wind farm in Brown County,Wisconsin. Report Number 122412-1.

[3] W. Richarz and H. Richarz "Wind turbine noise diagnostics" technical paper presented at Inter-noise, August 23-26 2009 Ottawa, Canada.

[4] A. Metelka "Narrowband low frequency pressure and vibration inside homes in proximity to wind farms" J. Acoust. Soc. Am., 134, 4097 (2013).

[5] J.R. Hassall and K. Zaveri "Acoustic Noise Measurements" Bruel & Kjaer, June 1988.

[6] J. D. Kester and G. F. Pickett "application of Theoretical Acoustics to the Reduction of Jet Engine Noise" 1972 Journal of applied physics Volume 5 number 1